# Resonant two-photon ionization spectroscopy of jet-cooled RuC

Jon D. Langenberg, Ryan S. DaBell, Lian Shao, Dawn Dreessen, and Michael D. Morse
*Department of Chemistry, University of Utah, Salt Lake City, Utah 84112*

(Received 1 June 1998; accepted 7 August 1998)

A resonant two-photon ionization study of the jet-cooled RuC molecule has identified the ground state as a $^1\Sigma^+$ state arising from the $10\sigma^2 11\sigma^2 5\pi^4 2\delta^4$ configuration. The $^3\Delta_i$ state arising from the $10\sigma^2 11\sigma^2 5\pi^4 2\delta^3 12\sigma^1$ configuration lies very low in energy, with the $^3\Delta_3$ and $^3\Delta_2$ components lying only 76 and 850 $cm^{-1}$ above the ground state, respectively. Transitions from the $X\ ^1\Sigma^+$, $^3\Delta_3$, and $^3\Delta_2$ states to the $^3\Pi_2$, $^3\Pi_1$, $^3\Phi_3$, $^3\Phi_4$, $^1\Phi_3$, and $^1\Pi_1$ states arising from the $10\sigma^2 11\sigma^2 5\pi^4 2\delta^3 6\pi^1$ configuration have been observed in the 12 700–18 100 $cm^{-1}$ range, allowing all of these states to be placed on a common energy scale. The bond length increases as the molecule is electronically excited, from $r_0 = 1.608$ Å in the $2\delta^4$, $X\ ^1\Sigma^+$ state, to 1.635 Å in the $2\delta^3 12\sigma^1$, $^3\Delta$ state, to 1.66 Å in the $2\delta^3 6\pi^1$, $^3\Pi$ and $^3\Phi$ states, to 1.667 Å in the $2\delta^3 6\pi^1$, $^1\Phi$ and 1.678 Å in the $2\delta^3 6\pi^1$, $^1\Pi$ state. A related decrease in vibrational frequency with electronic excitation is also observed. Hyperfine splitting is observed in the $2\delta^3 12\sigma^1$, $^3\Delta_3$ state for the $^{99}Ru(I=5/2)^{12}C$ and $^{101}Ru(I=5/2)^{12}C$ isotopic combinations. This is analyzed using known atomic hyperfine parameters to show that the $12\sigma$ orbital is roughly 83% $5s_{Ru}$ in character, a result in good agreement with previous work on the related RhC and CoC molecules. © *1998 American Institute of Physics.* [S0021-9606(98)01442-1]

## I. INTRODUCTION

In recent years there has been considerable interest in studying transition metal carbides using optical spectrometric techniques. Recent gas-phase work on these molecules include studies of FeC,[1–3] CoC,[4,5] YC,[6] NbC,[7] MoC,[8] IrC,[9] and PtC.[10,11] Additional work from our laboratory will be forthcoming on NiC (Ref. 12) and PdC.[13] There was an earlier period of interest in this type of molecule. Between the mid-sixties and the mid-seventies, conventional optical spectroscopic studies were performed on RhC,[14–16] IrC,[17,18] and PtC.[19–22] In addition to these optical studies, valuable information was garnered from matrix isolation electron spin resonance studies on VC,[23,24] NbC,[24] and RhC.[25] Over the past 15 years, the number of theoretical studies of the diatomic transition metal carbides has grown considerably as well, with published calculations reported for TiC,[26,27] VC,[28,29] CrC,[30,31] YC,[32] NbC,[7] MoC,[33] RuC,[34] RhC,[35–37] and IrC.[38]

Among the molecules studied in the early period was RuC. In 1971 Scullman and Thelin of the University of Stockholm recorded the emission spectrum of RuC from 6000 to 8700 Å.[39] The RuC molecules were produced by heating Ru powder in a graphite vessel to ~3000 °C in a King furnace. The emission spectrum was then recorded, first under low-dispersion conditions to survey the vibronic structure, and then under high-dispersion conditions to reveal the fine structure. They found 48 bands in this region, which were grouped into eight subsystems. Twelve of the most intense bands were rotationally analyzed to determine the spectroscopic constants. In 1972 the same investigators recorded an absorption spectrum of RuC from 4100 to 4800 Å under experimental conditions similar to their previous study, leading to the discovery of eight new bands and the confirmation that the lower state levels observed in emission could also be seen in absorption.[40]

Two experimental problems severely limited the knowledge that could be gained about RuC from the previous optical studies. First, many of the bands were complicated by overlapping lines from $C_2$, CN, and the different isotopomers of RuC. Second, the high temperatures required to produce RuC reduced the population in the low-$J$ levels, usually making the low-$J$ lines too weak to be detected. As a result, definitive $\Omega$-values could rarely be assigned to the observed bands. This precluded any serious attempts to understand the electronic structure of RuC, and provided the impetus for the present investigation. The present study employs a supersonic expansion source to produce rotationally cold molecules, allowing the first lines to be observed, and permitting definite $\Omega$-values to be assigned for the transitions. In addition, by using a mass spectrometric detection scheme, optical spectra could be independently collected for each isotopomer.

In addition to these spectroscopic investigations, a number of investigators have given their attention to the bond energy of RuC. McIntyre *et al.* measured the bond energy of RuC as $D_0 = 6.68 \pm 0.13$ eV by the third law method using Knudsen cell mass spectrometry.[41] Later, Gingerich used the same technique to measure the bond energy as $D_0 = 6.55 \pm 0.13$ eV.[42] Shim, Finkbeiner, and Gingerich subsequently recalculated this bond energy using an improved set of measurements and information from all-electron *ab initio* Hartree–Fock/configuration interaction calculations (HF/CI) as $D_0 = 6.34 \pm 0.11$ eV.[34] This value is an average of the second and third law determinations. The all-electron *ab initio* HF/CI calculations examined 28 electronic states, and predicted the ground state to be $^3\Delta$ with low-lying $^1\Sigma^+$ and $^1\Delta$ states.[34] A comparison of the results of the present spectro-

 

scopic study and these Hartree–Fock/configuration interaction results is presented in Sec. IV C below.

## II. EXPERIMENT

In this work the RuC molecule was investigated using resonant two-photon ionization (R2PI) spectroscopy performed on a supersonically cooled molecular beam with optical transitions detected mass spectrometrically. The RuC molecules were produced by focusing 532 nm radiation from a pulsed Nd:YAG laser to a 0.5 mm spot on a ruthenium–metal target disk. To remove metal uniformly, the target disk was rotated and translated side to side, driven by a system of gears, a cam, and a cam follower.[43] The ablation laser pulse was timed to coincide with a pulse of He carrier gas, seeded with approximately 3% methane, based on partial pressures. The carrier gas, along with the entrained atoms and molecules, expanded into a chamber maintained at $2\times10^{-4}$ Torr. The resulting molecular beam was roughly collimated by a skimmer and passed into a reflectron time-of-flight mass spectrometer, where it was probed by tunable radiation from a Nd:YAG-pumped dye laser or a Nd:YAG-pumped optical parametric oscillator/amplifier. Molecules absorbing this radiation were then ionized by 193 nm radiation from an excimer laser operating on an ArF mixture. The resulting ions were separated by mass and detected with a microchannel plate detector. The output from the detector was then amplified, digitized, and stored in a computer for later analysis. This entire experimental cycle was repeated at a rate of 10 Hz. No molecules other than RuC were observed in the mass spectra which were recorded, although the mass range above 120 Daltons was not carefully examined.

The spectrum of RuC was initially recorded with the dye laser in low resolution (0.7 $cm^{-1}$) to survey the vibronic bands. To study the fine structure of these bands, an étalon was placed in the dye laser cavity to narrow the linewidth (0.04 $cm^{-1}$), and the cavity was pressure scanned using Freon-12. To study the hyperfine structure of the $[12.7]^3\Pi_2\leftarrow[0.1]^3\Delta_3$ 0–0 band the narrow linewidth inherent in a Nd:YAG pumped optical parametric oscillator/amplifier (0.02 $cm^{-1}$) was used to record the spectrum. All of the rotationally resolved scans were calibrated by comparison to the well-known absorptions of $I_2$.[44–46]

To measure the lifetimes of the excited states, the excitation laser was tuned to the transition of interest, and the $RuC^+$ signal intensity monitored while the computer scanned the delay between the firing of the excitation and ionization lasers. In all cases the resulting curve was well-described as a single exponential decay. It was fit as such using a nonlinear least squares algorithm, permitting the $1/e$ lifetime to be extracted. The results of two or more separate lifetime measurements were averaged to obtain a final value. The lifetimes are listed in Table I for the upper states of the various bands.

## III. RESULTS

The spectrum of RuC from 11 975 to 18 400 $cm^{-1}$ and from 18 957 to 18 969 $cm^{-1}$ was recorded, resulting in the observation of approximately 49 bands, 29 of which were rotationally resolved and analyzed. The isotope shifts were determined by the difference between the fitted band origins of the $^{96}Ru^{12}C$ and the $^{104}Ru^{12}C$ isotopomers and are listed in Table I. The rotational structure of these bands was fit to the formula,

$$\nu=\nu_0+B'J'(J'+1)-B''J''(J''+1) \tag{3.1}$$

to yield values for $\nu_0$, $B'$, and $B''$. The results of these fits allowed the 29 bands to be grouped into nine subsystems, originating from three low-lying electronic states, $X\ ^1\Sigma^+$, $[0.1]^3\Delta_3$, and $[0.9]^3\Delta_2$. Throughout the remainder of this paper Hund's case (a) labels will be used to identify the observed states, along with the energies of the $v=0$ level of the state in question, in units of $10^3$ $cm^{-1}$. To exemplify this convention, the $^1\Phi_3$ state for which the $v=0$ level lies 16 195.145 $cm^{-1}$ above the $v=0$ level of the ground state is labeled as $[16.2]^1\Phi_3$. Justification for the Hund's case (a) labels that are suggested is provided in Sec. IV.

### A. Systems originating from the $X\ ^1\Sigma^+$ state

The determination of the $^1\Sigma^+$ term symbol, as well as its identification as the ground state, are discussed below. Somewhat surprisingly, no vibrational hot bands were observed arising from this state.

#### 1. The $[13.9]^3\Pi_1\leftarrow X\ ^1\Sigma^+$ system

The 0–0, 1–0, 2–0, and 3–0 vibrational bands were observed for this system, with vibrational numberings assigned based on isotope shifts. With the dye laser in low-resolution mode (0.7 $cm^{-1}$), the bands appear red-degraded with a small band gap. Under higher resolution the observation of $R(0)$, $Q(1)$, and $P(2)$ identifies the system as an $\Omega'=1\leftarrow\Omega''=0$ transition. For this band system lambda doubling in the $\Omega'=1$ upper state was included using the formula[47]

$$\nu=\nu_0+(B'\mp q'/2)J'(J'+1)-B''J''(J''+1), \tag{3.2}$$

where the upper sign is associated with $e$ levels of the upper state, the lower sign with $f$ levels. As justified below, it was assumed that the lower state is an $\Omega''=0^+$ state, which possesses only $e$ levels. As such, the upper sign was used for the $P$ and $R$ branches, which obey the selection rule $e\leftrightarrow e$, $f\leftrightarrow f$.[48] The lower sign was used for the $Q$ branch, which obeys the selection rule $e\leftrightarrow f$, $f\leftrightarrow e$.[48] Formula (3.2) is the accepted form for a $^3\Pi_1$ upper state,[47] which is in accord with the assignment suggested below. Spectroscopic constants derived for this system and all other rotationally resolved bands are given in Table I for $^{102}Ru^{12}C$. The measured rotational line positions for the various isotopomers of RuC for this and all other rotationally resolved bands are available from the author (M.D.M.) or the Physics Auxiliary Publication Service (PAPS).[49] This band system was not reported in the previous emission study of Scullman and Thelin,[39] although it certainly falls within the region investigated. Their failure to observe this system provides circumstantial evidence that the upper state is primarily triplet in character, making the $[13.9]^3\Pi_1\rightarrow X\ ^1\Sigma^+$ emission nominally spin-forbidden. If a spin-allowed emission pathway

TABLE I. Rotationally resolved vibronic bands of $^{102}Ru^{12}C$.[a]

| Band system | $v'-v''$ | $\nu_0$ ($cm^{-1}$) | $\Delta\nu_0$ ($cm^{-1}$)[b] | $B'_v$ ($cm^{-1}$) | $q'_v$ ($cm^{-1}$) | $B''_v$ ($cm^{-1}$) | $\tau$ ($\mu$s) |
|---|---|---|---|---|---|---|---|
| $[18.1]^1\Pi_1 \leftarrow X\ ^1\Sigma^+$ | 1–0 | 18 961.539 1(13) | 3.291 7(23) | 0.550 659(78) | −0.000 026(26) | 0.607 354(66) | 0.18(1) |
| | 0–0 | 18 086.015 7(29) | −0.426[c] | 0.555 115(95) | −0.000 108(86) | 0.607 354(66) | 0.19(1) |
| $[16.2]^1\Phi_3 \leftarrow [0.9]^3\Delta_2$ | 1–0 | 16 263.596 1(25) | 3.693 7(42) | 0.558 436(45) | | 0.587 106(46) | 0.43(3) |
| | 0–0 | 15 344.755 8(24) | −0.200 9(33) | 0.562 712(44) | | 0.587 106(46) | 0.45(5) |
| $[16.2]^1\Phi_3 \leftarrow [0.1]^3\Delta_3$ | 1–0 | 17 038.040 7(24) | 3.734 6(36) | 0.558 285(32) | | 0.585 528(40) | 0.50(7) |
| | 0–0 | 16 119.195 2(26) | −0.173 0(33) | 0.562 626(35) | | 0.585 528(40) | 0.45(7) |
| $[13.9]^3\Pi_1 \leftarrow X\ ^1\Sigma^+$ | 2–0 | 15 850.080 2(20) | 7.809 2(29) | 0.561 235(62) | 0.000 118(14) | 0.607 354(66) | 0.36(4) |
| | 1–0 | 14 902.947 8(20) | 3.821 5(30) | 0.565 367(49) | 0.000 038(36) | 0.607 354(66) | 0.36(5) |
| | 0–0 | 13 945.230 2(13) | −0.254 6(24) | 0.569 426(47) | 0.000 076(16) | 0.607 354(66) | 0.35(3) |
| $[13.9]^3\Pi_1 \leftarrow [0.9]^3\Delta_2$ | 2–0 | 14 999.690 4(19) | 7.980 6(29) | 0.560 930(50) | | 0.587 106(46) | 0.37(6) |
| | 1–0 | 14 052.556 7(21) | 4.003 2(23) | 0.565 046(34) | | 0.587 106(46) | 0.36(4) |
| | 0–0 | 13 094.844 4(16) | −0.074 7(23) | 0.569 082(41) | | 0.587 106(46) | 0.37(4) |
| $[13.9]^3\Phi_4 \leftarrow [0.1]^3\Delta_3$ | 3–1 | 15 589.219 9(32) | 7.227[c] | 0.555 005(52) | | 0.582 014(62) | 0.30(4) |
| | 2–1 | 14 667.153 2(27) | 3.396 1(48) | 0.559 268(86) | | 0.582 014(62) | 0.35(7) |
| | 1–1 | 13 734.217 6(32) | −0.530 1(43) | 0.563 453(71) | | 0.582 014(62) | 0.28(1) |
| | 2–0 | 15 696.758 1(27) | 7.782 3(55) | 0.559 012(38) | | 0.585 528(40) | 0.30(1) |
| | 1–0 | 14 763.810 2(25) | 3.857 0(50) | 0.563 247(58) | | 0.585 528(40) | 0.28(3) |
| | 0–0 | 13 820.116 2(37) | −0.159 8(55) | 0.567 392(60) | | 0.585 528(40) | 0.32(3) |
| $[13.5]^3\Phi_3 \leftarrow [0.9]^3\Delta_2$ | 0–0 | 12 624.318 9(18) | −0.156 3(28) | 0.565 241(50) | | 0.587 106(46) | 0.39(2) |
| $[13.5]^3\Phi_3 \leftarrow [0.1]^3\Delta_3$ | 2–1 | 14 238.097 8(30) | 3.383 7(41) | 0.556 957(82) | | 0.582 014(62) | 0.40(7) |
| | 1–1 | 13 309.255 5(28) | −0.518 6(41) | 0.561 239(66) | | 0.582 014(62) | 0.43(8) |
| | 1–0 | 14 338.838 9(18) | 3.869 0(33) | 0.560 969(43) | | 0.585 528(40) | 0.37(4) |
| | 0–0 | 13 398.745 9(25) | −0.128 0(41) | 0.565 129(40) | | 0.585 528(40) | 0.38(4) |
| $[12.7]^3\Pi_2 \leftarrow [0.1]^3\Delta_3$ | 3–1 | 14 500.038 1(27) | 7.659 5(54) | 0.558 449(86) | | 0.582 014(62) | 0.40(7) |
| | 2–1 | 13 553.173 6(34) | 3.716 0(41) | 0.561 308(64) | | 0.582 014(62) | 0.29(3) |
| | 1–1 | 12 596.055 3(30) | −0.307 5(45) | 0.566 158(84) | | 0.582 014(62) | |
| | 2–0 | 14 582.763 7(26) | 8.098 3(45) | 0.561 178(77) | | 0.585 528(40) | 0.31(3) |
| | 1–0 | 13 625.622 4(15) | 4.071 6(38) | 0.566 032(67) | | 0.585 528(40) | 0.31(1) |
| | 0–0 | 12 658.110 0(31) | −0.044 1(44) | 0.569 935(54) | | 0.585 528(40) | 0.34(1) |

[a]Bands originating from the same lower state were fitted simultaneously to reduce the correlation between the fitted $B'$ and $B''$ values. Numbers in parentheses represent $1\sigma$ error limits, in units of the last reported digits.

[b]The isotope shift is listed as $\Delta\nu_0 = \nu_0(^{96}Ru^{12}C) - \nu_0(^{104}Ru^{12}C)$.

[c]For this band an insufficient number of lines were identified for the $^{96}Ru^{12}C$ isotopomer, so the isotope shift $\Delta\nu_0 \equiv \nu_0(^{96}Ru^{12}C) - \nu_0(^{104}Ru^{12}C)$ is estimated by scaling the isotope shifts between the other isotopic combinations.

from the $[13.9]^3\Pi_1$ state were available, the branching ration for the $[13.9]^3\Pi_1 \rightarrow X\ ^1\Sigma^+$ emission process could well be negligible.

### 2. The $[18.1]^1\Pi_1 \leftarrow X\ ^1\Sigma^+$ system

Two vibrational bands belonging to this system were observed over the spectroscopic range investigated here; they were readily determined to be the 0–0 and the 1–0 bands on the basis of isotope shifts. Under low-resolution conditions, the 0–0 band appears red-degraded with no discernible band gap. A high resolution scan over the 1–0 band of this system for $^{102}Ru^{12}C$ is presented in Fig. 1. The branches are readily distinguished, and first lines of $R(0)$, $Q(1)$, and $P(2)$ identify the system as an $\Omega' = 1 \leftarrow \Omega'' = 0$ transition. As with the $[13.9]^3\Pi_1 \leftarrow X\ ^1\Sigma^+$ system, inclusion of a lambda doubling parameter for the upper state yielded a slight improvement in the fit. In this case, however, the fitting formula differed from Eq. (3.2) in the sign of $q'$, owing to the different conventions for $^3\Pi_1$ and $^1\Pi_1$ states.[47] Scullman and Thelin did not observe this band system because it appears between the regions of the spectrum that they photographed.[39,40]

## B. Systems originating from the $[0.1]^3\Delta_3$ state

The second set of band systems is generated from a $^3\Delta_3$ lower state. These band systems display vibrational hot bands, which permitted the $^3\Delta_3$ vibrational interval, $\Delta G_{1/2}$, to be accurately measured. A value of $\Delta G_{1/2} = 1029.587\ cm^{-1}$ was found for the $^{102}Ru^{12}C$ isotopomer.

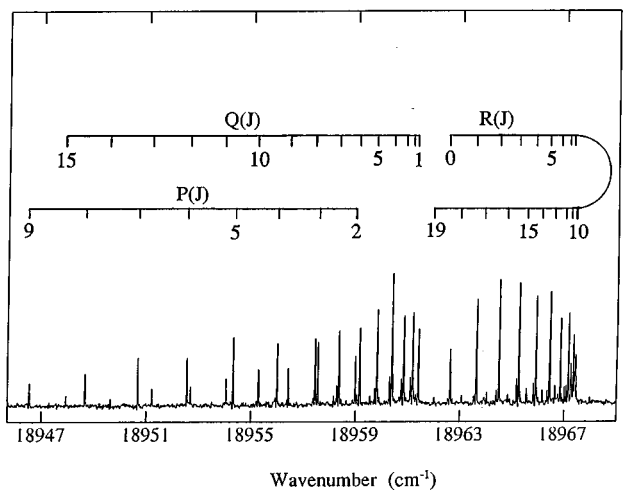


FIG. 1. Rotationally resolved scan over the 1–0 band of the $[18.1]^1\Pi_1 \leftarrow X\ ^1\Sigma^+$ system. This is fairly typical of the observed bands originating from the $X\ ^1\Sigma^+$ ground state, all of which terminate on $\Omega' = 1$ upper states.

### 1. The $[12.7]^3\Pi_2 \leftarrow [0.1]^3\Delta_3$ system

Under low resolution, a band system consisting of the 0–0, 1–0, 2–0, 1–1, 2–1, and 3–1 bands was recorded. The vibrational assignments were again based on isotope shifts and are unambiguous. Even at a resolution of 0.7 $cm^{-1}$, distinct branches are observed; the $Q$ branch is the most intense, followed by the $P$ and then the $R$ branches. Consistent with this intensity pattern and the large band gaps, the rotational structure was fit to the model of Eq. (3.1) as an $\Omega' = 2 \leftarrow \Omega'' = 3$ transition. The high-resolution spectra also revealed hyperfine splitting in $^{99}Ru(I = 5/2)^{12}C$ and $^{101}Ru(I = 5/2)^{12}C$. The analysis of the hyperfine structure is presented in Sec. III D. This system, designated the 7884 Å system, was observed in reasonable intensity by Scullman and Thelin, and the 0–0 band was rotationally analyzed; however, the hyperfine structure was unresolved.[39]

### 2. The $[13.5]^3\Phi_3 \leftarrow [0.1]^3\Delta_3$ system

Approximately 800 $cm^{-1}$ to the blue of the $[12.7]^3\Pi_2 \leftarrow [0.1]^3\Delta_3$ system lies another system consisting of 0–0, 1–0, 1–1, and 2–1 bands, with vibrational numberings again determined from isotope shifts. Under low-resolution, the bands appear red-degraded and exhibit distinct band gaps, with the $Q$ branch the most intense branch and with nearly equal intensity in the $P$ and $R$ branches. The intensity distribution in the branches and the large band gaps are indicative of a $\Delta\Omega = 0$ transition with a large value of $\Omega$. Upon detailed analysis, this is exactly what is found; the rotational structure of these bands could be well described by the model of Eq. (3.1) as an $\Omega' = 3 \leftarrow \Omega'' = 3$ transition. This band system also exhibited hyperfine broadening in $^{99}Ru^{12}C$ and $^{101}Ru^{12}C$.

A rotationally resolved scan of the 1–1 band of this system revealed a mysterious bump in the gap between the $R$ and $Q$ branches. The bump appeared in the same relative position in all of the isotopic combinations, reducing or ruling out the possibility that it arises from an impurity molecule. Comparing the position of this band with those recorded previously by Scullman and Thelin,[39] it was noticed that the position of a band they identified as the 0–0 band of the 7499 Å system came close, but was slightly higher in energy than the 1–1 band of our $[13.5]^3\Phi_3 \leftarrow [0.1]^3\Delta_3$ system. In fact, the low-$J$ lines of the $Q$ branch of the 0–0 band of the 7499 Å system, described by Scullman and Thelin, are in excellent agreement with the unresolved bump in our spectrum. This band was described as weak in the earlier work, and it was very weak in our spectra as well; nevertheless, the conditions that produced sharp peaks in the more intense 1–1 band of the $[13.5]^3\Phi_3 \leftarrow [0.1]^3\Delta_3$ system had power broadened the features of the $Q$ branch of the 0–0 band of the 7499 Å system so severely that only a single, broad feature was observed. The $[13.5]^3\Phi_3 \leftarrow [0.1]^3\Delta_3$ system was not observed in the emission spectra recorded by Scullman and Thelin.[39] This suggests, but does not prove, that the 7499 Å system obeys the $\Delta S = \Delta\Sigma = 0$ selection rule, but that this rule is broken in our observed $[13.5]^3\Phi_3 \leftarrow [0.1]^3\Delta_3$ system.

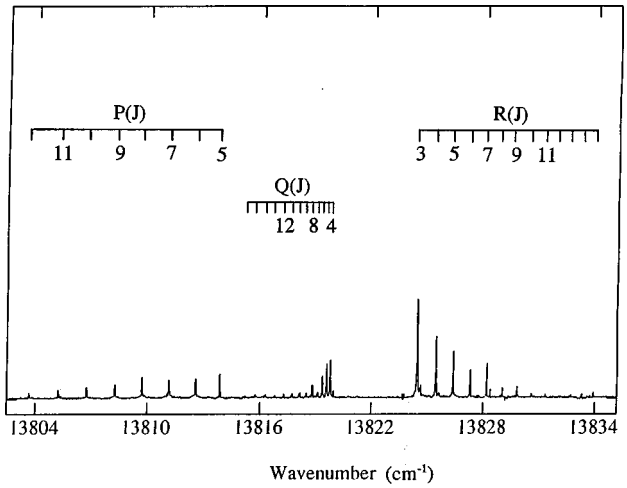


FIG. 2. Rotationally resolved scan over the 0–0 band of the $[13.9]^3\Phi_4 \leftarrow [0.1]^3\Delta_3$ system. The large gaps between the $R$, $Q$, and $P$ branches demonstrate that large values of $\Omega$ are involved in the transition; the first lines establish that $\Omega' = 4$ and $\Omega'' = 3$.

### 3. The $[13.9]^3\Phi_4 \leftarrow [0.1]^3\Delta_3$ system

The intense $[13.9]^3\Phi_4 \leftarrow [0.1]^3\Delta_3$ system provided the greatest number of observed bands. Transitions were observed from both $v'' = 0$ and 1 to $v' = 1-4$. Under low-resolution conditions, these bands appear with nearly equal intensity in the $Q$ and $R$ branches; however, the $P$ branch is greatly diminished in comparison with the other two branches, indicating that $\Delta\Omega = +1$ for this system. The gaps between the branches are quite wide as well, indicating that the values of $\Omega'$ and $\Omega''$ are large. A rotationally resolved scan over the 0–0 band of this system is displayed in Fig. 2. The existence of $P$, $Q$, and $R$ branches with first lines of $R(3)$, $Q(4)$, and $P(5)$ identify the system as an $\Omega' = 4 \leftarrow \Omega'' = 3$ system, in agreement with the arguments based on the low resolution spectrum. The $^{99}Ru^{12}C$ and $^{101}Ru^{12}C$ isotopomers exhibited hyperfine broadening, which was not resolvable at a resolution of 0.04 $cm^{-1}$. This system was observed in the earlier work of Scullman and Thelin, designated as the 7224 Å system, and 5 bands were rotationally resolved.[39] It was the most intense band system observed in emission, consistent with its high intensity in absorption in the present study.

### 4. The $[16.2]^1\Phi_3 \leftarrow [0.1]^3\Delta_3$ system

This system consists of a 0–0 band and a 1–0 band. Under low-resolution conditions the bands appeared with distinct well-separated branches, the $R$ and $P$ branches nearly equal in intensity and nearly equally spaced from the more intense $Q$ branch. Fitting the rotationally resolved spectra of these bands revealed them to be $\Omega' = 3 \leftarrow \Omega'' = 3$ transitions. The $^{99}Ru^{12}C$ and $^{101}Ru^{12}C$ isotopomers were again broadened by hyperfine interactions, but the hyperfine splittings could not be resolved in the present study. This band system was not observed in the emission study of Scullman and Thelin,[39] again suggesting that it is a spin-forbidden transition.

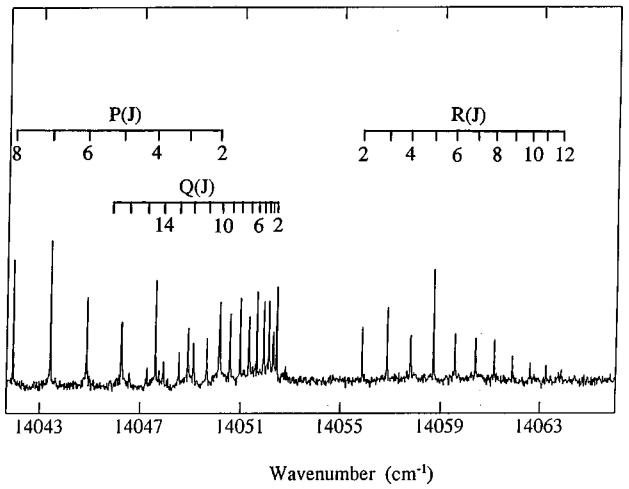


FIG. 3. Rotationally resolved scan over the 1–0 band of the $[13.9]^3\Pi_1 \leftarrow [0.9]^3\Delta_2$ system.

### C. Systems originating from the $[0.9]^3\Delta_2$ state

The third low-lying state, identified below as the $[0.9]^3\Delta_2$ state, allowed us to place the other states on a common energy scale. No hot bands could be found originating from this state.

#### 1. The $[13.5]^3\Phi_3 \leftarrow [0.9]^3\Delta_2$ system

Only a single band belonging to this system was observed. Under low resolution three distinct branches were evident. They displayed a slight shading to the red, with the intensity of the $R$ branch nearly equal to that of the $Q$ branch. The $P$ branch is weak compared to the other branches. Observation of the first lines identified the band as an $\Omega' = 3 \leftarrow \Omega'' = 2$ transition. This system, designated as the 7909 Å system, was also observed weakly in the emission spectra recorded by Scullman and Thelin, who rotationally analyzed the 0–0 band.[39]

#### 2. The $[13.9]^3\Pi_1 \leftarrow [0.9]^3\Delta_2$ system

This system consists of a progression from the $v'' = 0$ level to the $v' = 0$, 1, 2, and 3 levels. At lower resolution, the peaks appear red-degraded with a band gap between the $R$ and $Q$ branches, the $Q$ branch being the more intense of the two. It is difficult to determine where the $P$ branch begins and the $Q$ branch ends; therefore, it is difficult to gauge their relative intensities in the low resolution scans. A rotationally resolved scan over the 1–0 band of this system for $^{102}Ru^{12}C$ is displayed in Fig. 3. This demonstrates the first lines of $R(2)$, $Q(2)$, and $P(2)$, which identify the system as an $\Omega' = 1 \leftarrow \Omega'' = 2$ electronic transition. This system, designated as the 7623 Å system, was also recorded in the emission study of Scullman and Thelin.[39] In emission it appears as a fairly strong system.

#### 3. The $[16.2]^1\Phi_3 \leftarrow [0.9]^3\Delta_2$ system

Only two members of the $[16.2]^1\Phi_3 \leftarrow [0.9]^3\Delta_2$ system were observed in this study, the 0–0 and the 1–0 bands. Under low resolution conditions these bands are marked by three distinct branches, with the $Q$ branch the most intense followed by the $R$ and then the $P$. Like the other bands in this study, these bands are slightly red-degraded. Under higher resolution the bands are readily identified as $\Omega' = 3 \leftarrow \Omega'' = 2$ transitions from the first lines, $R(2)$, $Q(3)$, and $P(4)$. This system, designated as the 6509 Å system, was previously observed quite weakly in the emission spectra recorded by Scullman and Thelin.[39]

This band system, along with the $[13.9]^3\Pi_1 \leftarrow [0.9]^3\Delta_2$ system, allowed the $^1\Sigma^+$, $^3\Delta_3$, and $^3\Delta_2$ states to be placed on a common energy scale. The measured upper state vibrational intervals and rotational constants, listed in Table II, establish that the $[16.2]^1\Phi_3 \leftarrow [0.9]^3\Delta_2$ and $[16.2]^1\Phi_3 \leftarrow [0.1]^3\Delta_3$ systems share a common upper state. Likewise, the $[13.5]^3\Phi_3 \leftarrow [0.9]^3\Delta_2$ and the $[13.5]^3\Phi_3 \leftarrow [0.1]^3\Delta_3$ systems certainly share a common upper state. The values of $B'$ and $\Delta G'$ for the $[13.9]^3\Pi_1 \leftarrow [0.9]^3\Delta_2$ and the $[13.9]^3\Pi_1 \leftarrow X\ ^1\Sigma^+$ systems, also listed in Table II, likewise demonstrate that these systems share a common upper state. Subtracting corresponding band origins for the systems having a common upper state then allows the lower states to be placed on the same energy scale. The final result is that the $^1\Sigma^+$ term is the ground state with the $v = 0$ level of the $^3\Delta_3$ term lying 75.953 $cm^{-1}$ above the $v = 0$ level of the $^1\Sigma^+$ term for $^{102}Ru^{12}C$. The $v = 0$ level of the $^3\Delta_2$ term then lies 850.386 $cm^{-1}$ above the $v = 0$ level of the $^1\Sigma^+$ term for $^{102}Ru^{12}C$. Transitions that correspond to the $[18.1]^1\Pi \leftarrow [0.9]^3\Delta_2$ system were also observed ~850 $cm^{-1}$ to the

TABLE II. Bands linking the $X\ ^1\Sigma^+$, $[0.1]^3\Delta_3$, and $[0.9]^3\Delta_2$ states of $^{102}Ru^{12}C$.[a]

| Linked states | Band system | $B'_0$ | $B'_1$ | $B'_2$ | $\Delta G'_{1/2}$ | $\Delta G'_{3/2}$ |
|---|---|---|---|---|---|---|
| $X\ ^1\Sigma^+$,$[0.9]^3\Delta_2$ | $[13.9]^3\Pi_1 \leftarrow X\ ^1\Sigma^+$ | 0.569 43(5)[b] | 0.565 37(5)[b] | 0.561 24(6)[b] | 957.718(2) | 947.132(3) |
| | $[13.9]^3\Pi_1 \leftarrow [0.9]^3\Delta_2$ | 0.569 08(4)[b] | 0.565 05(3)[b] | 0.560 93(5)[b] | 957.712(3) | 947.134(3) |
| $[0.9]^3\Delta_2$,$[0.1]^3\Delta_3$ | $[16.2]^1\Phi_3 \leftarrow [0.1]^3\Delta_3$ | 0.562 63(4) | 0.558 28(3) | | 918.846(4) | |
| | $[16.2]^1\Phi_3 \leftarrow [0.9]^3\Delta_2$ | 0.562 71(4) | 0.558 44(5) | | 918.840(3) | |
| | $[13.5]^3\Phi_3 \leftarrow [0.1]^3\Delta_3$ | 0.565 13(4) | | | | |
| | $[13.5]^3\Phi_3 \leftarrow [0.9]^3\Delta_2$ | 0.565 24(5) | | | | |

[a]All values are in $cm^{-1}$. Numbers in parentheses provide the $1\sigma$ error limits, in units of 0.000 01 $cm^{-1}$ for $B$ values and 0.001 $cm^{-1}$ for $\Delta G$ values.

[b]The systematic discrepancy between the rotational constants of the $[13.9]^3\Pi_1$ state as measured from the $[13.9]^3\Pi_1 \leftarrow X\ ^1\Sigma^+$ vs the $[13.9]^3\Pi_1 \leftarrow [0.9]^3\Delta_2$ band systems is likely due to the fact that the lambda doublets of the $[13.9]^3\Pi_1 \leftarrow [0.9]^3\Delta_2$ system were not resolved, while the lines of the $[13.9]^3\Pi_1 \leftarrow X\ ^1\Sigma^+$ system are not doubled. The good agreement found in comparing $B'$ and $\Delta G'$ values measured in the different systems for the $^{102}Ru^{12}C$ isotopic modification demonstrates that the different systems do indeed terminate on the same upper state. Similar agreement is found when the corresponding values of $B'$ and $\Delta G'$ are compared for other isotopic combinations.

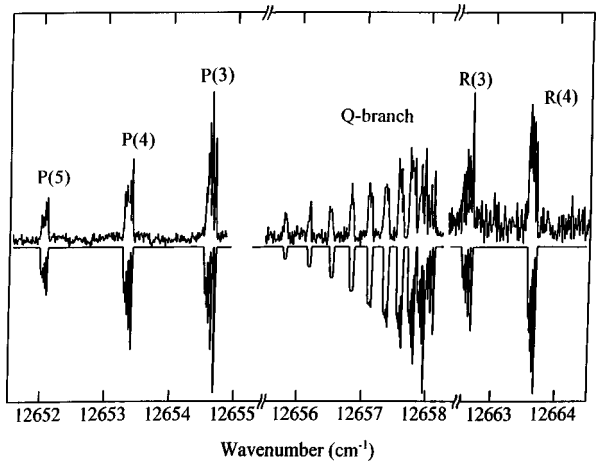


FIG. 4. The hyperfine splitting in the low-$J$ lines of the $[12.7]^3\Pi_2 \leftarrow [0.1]^3\Delta_3$ transition. The upper trace is the measured spectrum at 0.02 $cm^{-1}$ resolution; the lower trace is the inverted simulated spectrum. Note the breaks in the scale at 12 655 and 12 658 $cm^{-1}$.

red of the corresponding $[18.1]^1\Pi \leftarrow X\ ^1\Sigma^+$ system; the transitions were too weak for rotationally resolved studies, however.

### D. Hyperfine structure of the rotationally resolved bands

The $^{99}$Ru and $^{101}$Ru isotopes have magnetic nuclei ($I=5/2$) and as a result $^{99}Ru^{12}C$ and $^{101}Ru^{12}C$ can exhibit hyperfine splitting in their rotationally resolved spectra. In all of the spectra recorded here, the hyperfine splitting found for $^{101}Ru^{12}C$ is slightly larger than that found for $^{99}Ru^{12}C$, a result which is consistent with the $^{101}$Ru and $^{99}$Ru $g$-values of $-0.272$ and $-0.248$, respectively.[50] The band system that exhibits the largest hyperfine splitting is the $[12.7]^3\Pi_2 \leftarrow [0.1]^3\Delta_3$ system, displayed in Fig. 4. For the low $J$ lines, most of the hyperfine structure is resolved; however, the magnitude of the splitting decreases rapidly as $J$ increases, and the hyperfine lines become unresolved at higher $J$. While the hyperfine envelope of the $[13.9]^3\Phi_4 \leftarrow [0.1]^3\Delta_3$ system is as broad as it is for the $[12.7]^3\Pi_2 \leftarrow [0.1]^3\Delta_3$ system, the lines are mostly unresolved. For the remaining systems that exhibit hyperfine splitting, the $[13.5]^3\Phi_3 \leftarrow [0.1]^3\Delta_3$, $[16.2]^1\Phi_3 \leftarrow [0.1]^3\Delta_3$, and $[16.2]^1\Phi_3 \leftarrow [0.9]^3\Delta_2$ systems, the lines are merely broadened with partial resolution at best.

Because of the large spin–orbit effects expected in RuC ($\zeta_{4d}(\mathrm{Ru}) \approx 1038\ cm^{-1}$),[48] all of the states involved in the observed transitions are expected to belong to Hund's case (a), possibly showing significant spin–orbit mixing with other Hund's case (a) states. In such cases the hyperfine levels are expected to follow the formulas developed by Frosch and Foley for the $a_\beta$ coupling case,[51] in which the electronic angular momenta $\hat{\mathbf{L}}$ and $\hat{\mathbf{S}}$ have well-defined projections on the molecular axis, $\Lambda$ and $\Sigma$, respectively, and the total angular momentum apart from nuclear spin, $J$, defines the rotational energy levels according to Eq. (3.1). Coupling of $\hat{\mathbf{J}}$ with the nuclear spin, $\hat{\mathbf{I}}$, then leads to the total angular momentum, $\hat{\mathbf{F}}$, with the hyperfine contribution to the energy given by[51]

$$E_{\mathrm{hf}}(S,\Lambda,\Sigma,\Omega,I,J,F) = h\Omega\left[\frac{F(F+1)-I(I+1)-J(J+1)}{2J(J+1)}\right] \tag{3.3}$$

to first order in perturbation theory. In this formula

$$h = a\Lambda + (b_F + \tfrac{2}{3}c)\Sigma, \tag{3.4}$$

where

$$a = 2.000 g_I \beta_e \beta_n \langle r^{-3}\rangle, \tag{3.5}$$

$$b_F = g_e g_I \beta_e \beta_n \frac{8\pi}{3} |\psi(0)|^2, \tag{3.6}$$

and

$$c = \tfrac{3}{2} g_e g_I \beta_e \beta_n \langle 3\cos^2\theta - 1\rangle \langle r^{-3}\rangle. \tag{3.7}$$

Here $g_e = 2.002\ 319\ 3$ is the electronic $g$-factor;[50] $g_I \equiv \mu_I/I$ is the nuclear $g$-factor, given by the nuclear magnetic dipole moment in nuclear magnetons divided by the nuclear spin, $I$; $\beta_e$ is the Bohr magneton; $\beta_n$ is the nuclear magneton; $\theta$ is the angle between the internuclear axis and the vector from the magnetic nucleus to the electron; the expectation values provide averages for the single unpaired electron; and $|\psi(0)|^2$ provides the probability density for finding the electron at the magnetic nucleus. The numerical factors $g_e\beta_e\beta_n$ combine to give the value 0.003 186 $cm^{-1}$ $bohr^3$.[50]

Formulas (3.4)–(3.7) are appropriate for a single electron outside of closed shells, and must be generalized for the case of more than one electron. The resulting expression is given by[52,53]

$$h = \left\langle \sum_i \left[ a_i \hat{l}_{z,i} + (b_{Fi} + \tfrac{2}{3}c_i)\hat{s}_{z,i}\right]\right\rangle, \tag{3.8}$$

where the sum is over all electrons outside of closed shells, with $\hat{l}_{z,i}$ and $\hat{s}_{z,i}$ giving the projections of electronic orbital and spin angular momentum on the axis for electron $i$. The parameters $a_i$, $b_{Fi}$, and $c_i$ are then given by Eqs. (3.5)–(3.7), with the expectation values and $|\psi(0)|^2$ evaluated for electron $i$.

For transition metal systems with unpaired electron density in orbitals with significant $s$ character on the transition metal atom, $h$ is dominated by the Fermi contact term, $b_F$, which is typically a factor of 10 larger than either $a$ or $c$. A valid rough approximation, therefore, is to assume that any case ($a_\beta$) state with $\Sigma = 0$ will display negligible hyperfine splitting. This assumption provided the starting point for our analysis of the hyperfine structure of the RuC molecule.

Because $\Sigma = 0$ in the $[0.9]^3\Delta_2$ state there can be no Fermi contact contribution to $h$, and its hyperfine splitting will be small. The fact that the $[13.5]^3\Phi_3 \leftarrow [0.9]^3\Delta_2$ system does not exhibit hyperfine splitting therefore implies that the $[13.5]^3\Phi_3$ state has a small hyperfine splitting as well. However, the $[13.5]^3\Phi_3 \leftarrow [0.1]^3\Delta_3$ system does exhibit hyperfine splitting, which must therefore be primarily attributed to the lower $[0.1]^3\Delta_3$ state. To estimate this splitting, spectral simulations were performed for $^{101}Ru^{12}C$ using laser linewidths and rotational temperatures estimated from simulations of the simultaneously recorded $^{102}Ru^{12}C$ spectrum, which is free of hyperfine effects. From this the parameter

TABLE III. Electronic states of $^{102}Ru^{12}C$ below 18 300 $cm^{-1}$.[a]

| State | $T_0$ ($cm^{-1}$) | $\omega_e$ ($cm^{-1}$) | $\omega_e x_e$ ($cm^{-1}$) | $B_e$ ($cm^{-1}$)[b] | $\alpha_e$ ($cm^{-1}$) | $r_e$ (Å)[b] | $h$ ($cm^{-1}$) | $\tau$ ($\mu$s) |
|---|---|---|---|---|---|---|---|---|
| $[18.1]^1\Pi_1$ | 18 086.016 | $\Delta G_{1/2}=875.523$ | | 0.557 343 | 0.004 456 | 1.678 50 | | 0.18(1) |
| $[16.2]^1\Phi_3$[c] | 16 195.145(4) | $\Delta G_{1/2}=918.843(4)$ | | 0.564 823(130) | 0.004 308(123) | 1.667 34(19) | −0.018(3) | 0.44(2) |
| $^3\Pi_{0b}$[d] | $x+13\ 312.69$[d] | $\Delta G_{1/2}\approx 962$[d] | | $B_0=0.570\ 1(7)$[d] | | $r_0=1.660\ 3(10)$[d] | | |
| $^3\Pi_{0a}$[d] | $x+13\ 286.43$[d] | $\Delta G_{1/2}\approx 949$[d] | | $B_0=0.569\ 7(14)$[d] | | $r_0=1.660\ 9(20)$[d] | | |
| $^3\Phi_2$[d] | $x+12\ 875.23$[d] | $\Delta G_{1/2}\approx 944$[d] | | $B_0=0.569\ 1(4)$[d] | | $r_0=1.661\ 8(6)$[d] | | |
| $[13.9]^3\Pi_1$ | 13 945.230 | 968.297(8) | 5.291(3) | 0.571 310(210) | 0.004 086(158) | 1.657 85(30) | | 0.36(2) |
| $[13.9]^3\Phi_4$ | 13 896.059(24) | 954.544(46) | 5.408(11) | 0.569 517(140) | 0.004 144(92) | 1.660 46(20) | | 0.29(1) |
| $[13.5]^3\Phi_3$[c] | 13 474.699 | 951.344 | 5.625 | 0.567 249(136) | 0.004 109(110) | 1.663 77(20) | 0.000(3) | 0.39(2) |
| $[12.7]^3\Pi_2$ | 12 734.073(24) | 977.818(46) | 5.165(11) | 0.571 873(624) | 0.004 015(411) | 1.657 04(90) | 0.008(5) | 0.32(1) |
| $^3\Delta_1$[d] | $x\approx 1900$ | $\Delta G_{1/2}\approx 1032$[d] | | $B_0=0.588\ 4$[d] | | $r_0=1.634\ 3$[d] | | |
| $[0.9]^3\Delta_2$ | 850.386 | | | $B_0=0.587\ 106(46)$ | | $r_0=1.635\ 40(6)$ | 0.000(5) | |
| | | 1039.14(36)[e] | 4.75(16)[e] | | | | | |
| $[0.1]^3\Delta_3$ | 75.953 | | | 0.587 285 | 0.003 514 | 1.635 15 | −0.030(3) | |
| | | $\Delta G_{1/2}=1\ 029.587(20)$[f] | | | | | | |
| $X\ ^1\Sigma^+$ | 0.000 | | | $B_0=0.607\ 354(66)$ | | $r_0=1.607\ 90(9)$ | | |

[a]Numbers in parentheses indicate the $1\sigma$ error limits of the indicated quantity, in units of the last digits quoted. Additional higher energy excited electronic states are also known from the absorption spectra of RuC reported in the 410–480 nm region by R. Scullman and B. Thelin, Phys. Scr. **5**, 201 (1972).

[b]Because of possible *L*- and *S*-uncoupling interactions with other states, all *B*-values should be considered as effective-*B* values. The unknown magnitude of these interactions introduces an uncertainty into the conversion of *B*-values to bond lengths. Because the density of electronic states is fairly low, however, the bond lengths obtained for the $X\ ^1\Sigma^+$, $[0.1]^3\Delta_3$, and $[0.9]^3\Delta_2$ states are probably correct to within 0.001 Å. The uncertainties in bond lengths arising from the effects of *L*- and *S*-uncoupling interactions could be larger for the higher lying states, however.

[c]The $[16.2]^1\Phi_3$ and $[13.5]^3\Phi_3$ states are certainly strongly mixed, and the spin multiplicity is poorly defined for these states.

[d]Data taken from R. Scullman and B. Thelin, Phys. Scr. **3**, 19 (1971). From the data currently available, it is impossible to identify the $^3\Pi\ \Omega=0^+$ and $\Omega=0^-$ components. The assignment of the $^3\Phi_2$, $^3\Pi_{0a}$, $^3\Pi_{ob}$, and $^3\Delta_1$ states is reasonable but unproven at this time. The reported rotational constants are averaged over the isotopic contributors for $Ru^{12}C$, as are the estimates of $\Delta G_{1/2}$. In addition, the estimates of $\Delta G_{1/2}$ are based on band heads, rather than on fitted values of $\nu_0$. Calculated $r_0$ values are based on the averaged reduced mass of the $Ru^{12}C$ molecule.

[e]These data were taken from R. Scullman and B. Thelin, Phys. Scr. **3**, 19 (1971).

[f]This work.

$h''\Omega''$ was estimated as $h''\Omega''=-0.09\ cm^{-1}$ for the $[0.1]^3\Delta_3$ state. Using this value in the simulation of the $[12.7]^3\Pi_2 \leftarrow [0.1]^3\Delta_3$ system, $h'\Omega'$ was determined as $0.016\ cm^{-1}$ for the $[12.7]^3\Pi_2$ state. A comparison of the simulated and measured spectra for this system is given in Fig. 4. The lack of hyperfine effects in the $[13.5]^3\Phi_3 \leftarrow [0.9]^3\Delta_2$ system also implies that the hyperfine splitting in the $[16.2]^1\Phi_3 \leftarrow [0.9]^3\Delta_2$ system arises from the upper state of the transition. Simulating this spectrum yielded an $h'\Omega'$ parameter of $-0.055\ cm^{-1}$ for the $[16.2]^1\Phi_3$ state. Combining this upper state parameter with the lower state parameter obtained from the $[13.5]^3\Phi_3 \leftarrow [0.1]^3\Delta_3$ system allowed us to predict the hyperfine splitting in the $[16.2]^1\Phi_3 \leftarrow [0.1]^3\Delta_3$ system, thereby testing the values of $h\Omega$ for consistency. The predicted hyperfine broadening was slightly less than that observed in the measured spectrum, but the overall level of agreement was sufficient to trust our values of $h\Omega$ for the various states to an accuracy of roughly $\pm 0.01\ cm^{-1}$. The values of $h$ obtained for the various states are provided in Table III, along with a summary of the spectroscopic properties of all of the states of $^{102}Ru^{12}C$.

### E. Ionization energy of RuC

In their Knudsen effusion mass spectrometric study, McIntyre *et al.* could not determine the appearance potential of RuC due to low signal strength.[41] In the present investigation, however, the ionization energy, IE(RuC), is found to lie between 6.42 eV and 8.01 eV. The lower limit of 6.42 eV was established because resonant enhancement of the $RuC^+$ signal was observed using ArF excimer radiation for excitation, thereby proving that the molecule was not ionized by one photon of the ArF laser. The upper limit of 8.01 eV was established by combining the ArF photon energy with the energy of the $v=0$ level of the $[12.7]^3\Pi_2$ state, which is the lowest upper state energy level which is known to be ionized by ArF radiation. A minor correction is also made to account for the shift in the ionization threshold due to the field ionization effect. From this bracketing of the RuC ionization energy we find $IE(RuC)=7.22\pm0.80$ eV. Although the error limits of this measurement are quite large, it nevertheless provides the only estimate of the RuC ionization energy to date.

Using this value of IE(RuC) it is possible to derive limits on the bond energy of $RuC^+$ by making use of the thermodynamic cycle

$$D_0(RuC^+)=IE(Ru)+D_0(RuC)-IE(RuC). \tag{3.9}$$

The IE of the Ru atom is $59\ 366.4\pm0.3\ cm^{-1}=7.360$ eV.[54] The bond energy of RuC was determined by Shim *et al.* using Knudsen effusion mass spectrometry to be $6.34\pm0.11$ eV (Ref. 34) and this value is revised below to $6.31\pm0.11$ eV. Combining these values with the present range for IE(RuC) we obtain $D_0(RuC^+)=6.45\pm0.81$ eV.

## IV. DISCUSSION

To a first approximation, the bonding in RuC may be understood in terms of a molecular orbital diagram as shown in Fig. 5. Considering only the valence $4d_{Ru}$, $5s_{Ru}$, $2s_C$, and $2p_C$ atomic orbitals, one expects to find four low-lying orbitals ($10\sigma$, $11\sigma$, and the doubly degenerate $5\pi$ orbital

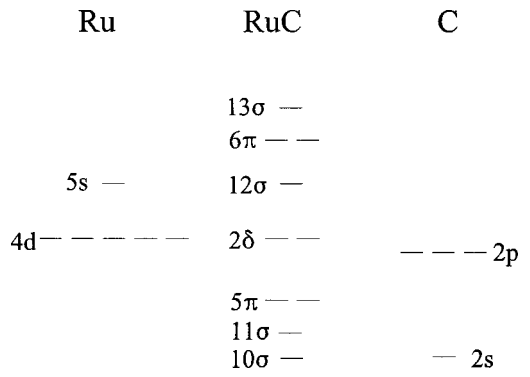


FIG. 5. Schematic molecular orbital diagram for RuC.

pair). These are probably filled in all of the states observed in this work. In one limiting viewpoint the $2s_C$ atomic orbital may be considered to be corelike, becoming the nonbonding $10\sigma$ orbital in the RuC molecule. Above this lies the bonding $11\sigma$ orbital, which is primarily a mix of $2p\sigma_C$ and $4d\sigma_{Ru}$. This is followed by the bonding $5\pi$ orbital, which is a mix of $2p\pi_C$ and $4d\pi_{Ru}$. Next come the $2\delta$ and $12\sigma$ orbitals, which by comparison to the better known metal oxides are thought to be primarily nonbonding in character. The $2\delta$ orbitals are almost purely $4d\delta_{Ru}$ in character, owing to the lack of energetically accessible $\delta$ orbitals on the carbon atom. The $12\sigma$ orbital is thought to be primarily $5s\sigma_{Ru}$ in character. At substantially higher energies one expects to find the antibonding $6\pi$ and $13\sigma$ orbitals, which are expected to be primarily combinations of the $4d\pi_{Ru}+2p\pi_C$ and $4d\sigma_{Ru}+2p\sigma_C$ orbitals, respectively.

The opposite limiting viewpoint considers that fact that the $2s$ and $2p$ orbitals of carbon are rather close in energy, causing them to mix to form *sp* hybrid orbitals. One of these points toward the metal atom and forms bonding and antibonding combinations with the $4d\sigma_{Ru}$ orbital. The other points away from the metal and is primarily nonbonding. Apart from the energy ordering of the $10\sigma$, $11\sigma$, and $5\pi$ orbitals, these two views lead to rather similar expectations for the higher energy orbitals, making them hard to distinguish in practice. In addition, both suffer from the defect that they ignore the effects of configuration interaction, which limits the validity of the molecular orbital picture.

### A. Low energy states of RuC: $X\ ^1\Sigma^+$, $[0.1]^3\Delta_3$, and $[0.9]^3\Delta_2$

The lowest energy states of RuC, a 12 valence electron species, certainly derive from configurations in which the $10\sigma$, $11\sigma$, and $5\pi$ orbitals are filled. The remaining 4 electrons are then presumably distributed among the nonbonding $2\delta$ and $12\sigma$ orbitals. In recent work NbC has been shown to have a ground state of $X\ ^2\Delta_{3/2}$, derived from a $10\sigma^2 11\sigma^2 5\pi^4 2\delta^1$ configuration, although the $10\sigma^2 11\sigma^2 5\pi^4 12\sigma^1$, $^2\Sigma^+$ state was found to lie only 830 $cm^{-1}$ higher in energy.[7] Likewise, the ground state of MoC is calculated to be the $10\sigma^2 11\sigma^2 5\pi^4 2\delta^2$, $^3\Sigma^-$ state, as is experimentally observed,[8] with the $10\sigma^2 11\sigma^2 5\pi^4 2\delta^1 12\sigma^1$, $^3\Delta$ state calculated to lie some 4500 $cm^{-1}$ higher in energy.[33] Given that the $2\delta$ and $12\sigma$ orbitals are primarily metal $4d$ and $5s$ in character, the greater stabilization of the $4d$ orbitals as one moves to larger nuclear charge suggests that the $2\delta$ orbitals will be even further stabilized as one moves to RuC. Thus the lowest energy configurations expected in RuC are $10\sigma^2 11\sigma^2 5\pi^4 2\delta^4$ and $10\sigma^2 11\sigma^2 5\pi^4 2\delta^3 12\sigma^1$, resulting in low energy molecular terms of $^1\Sigma^+$ and $^3\Delta_i$, respectively. The lowest spin–orbit levels expected are $\Omega=0^+$ (from $10\sigma^2 11\sigma^2 5\pi^4 2\delta^4$, $^1\Sigma^+$) and $\Omega=3$ (from $10\sigma^2 11\sigma^2 5\pi^4 2\delta^3 12\sigma^1$, $^3\Delta_i$), with $\Omega=2$ and $\Omega=1$ (also from $10\sigma^2 11\sigma^2 5\pi^4 2\delta^3 12\sigma^1$, $^3\Delta_i$) lying somewhat higher in energy.

These expectations are in perfect accord with the observed states. An $\Omega=0$ state lies lowest in energy, with an $\Omega=3$ state 75.953 $cm^{-1}$ higher in energy and an $\Omega=2$ level 850.386 $cm^{-1}$ above the ground $\Omega=0$ level. The correspondence between the expected levels and the observed levels allows the low-energy $\Omega=0$, 3, and 2 levels to be assigned to the $10\sigma^2 11\sigma^2 5\pi^4 2\delta^4$, $^1\Sigma^+(0^+)$; $10\sigma^2 11\sigma^2 5\pi^4 2\delta^3 12\sigma^1$, $^3\Delta_3$; and $10\sigma^2 11\sigma^2 5\pi^4 2\delta^3 12\sigma^1$, $^3\Delta_2$ states, respectively. At energies of ~2150 and 5200 $cm^{-1}$ one may expect to find the $10\sigma^2 11\sigma^2 5\pi^4 2\delta^3 12\sigma^1$, $^3\Delta_1$ and $10\sigma^2 11\sigma^2 5\pi^4 2\delta^3 12\sigma^1$, $^1\Delta_2$ states, respectively, as is derived in the next paragraph.

The measured separation between the $\Omega=3$ and 2 levels of RuC implies a value of $A\Lambda=-774.43$ $cm^{-1}$ for the $^3\Delta_i$ state. For a $2\delta^3 12\sigma^1$, $^3\Delta_i$ state the spin–orbit constant, $A$, is related to the microscopic spin–orbit parameter, $a_\delta$, as $A=-a_\delta/2$. Furthermore, since the $2\delta$ orbital is purely $4d\delta_{Ru}$ in character, $a_\delta=\zeta_{4d}(Ru)\approx 1038$ $cm^{-1}$.[48] Thus, a value of $A\Lambda=-1038$ $cm^{-1}$ might be expected for the $^3\Delta_i$ state of RuC. This would suggest that the $^3\Delta_1$ $v=0$ level should lie roughly $2\times 1038$ $cm^{-1}$ above the $^3\Delta_3$ $v=0$ level, or roughly 2152 $cm^{-1}$ above the $X\ ^1\Sigma^+$ $v=0$ level. The uneven intervals between the $\Omega=3$, 2, and 1 levels of the $^3\Delta_i$ state are expected to result primarily from an off-diagonal spin–orbit matrix element that connects the $^3\Delta_2$ and $^1\Delta_2$ states deriving from the same $2\delta^3\ 12\sigma^1$ configuration. This matrix element is easily calculated,[48] and is found to be $-\zeta_{4d}(Ru)\approx -1038$ $cm^{-1}$. Using this value and the fact that the $^3\Delta_2$ $v=0$ level lies 264 $cm^{-1}$ lower than expected, it is possible to solve for the location of the perturbing $^1\Delta_2$ $v=0$ level, which is thereby predicted to lie 4350 $cm^{-1}$ above the $^3\Delta_2$, $v=0$ level, at an energy of 5202 $cm^{-1}$ above the $X\ ^1\Sigma^+$ $v=0$ level. The predicted separation between the $^1\Delta_2$ and $^3\Delta_2$ states of 4350 $cm^{-1}$ is in rough agreement with what might be expected based on the separations between high-spin and low-spin atomic states. For example, after averaging over spin–orbit levels the $4d^7(^4F)5s^1$, $^3F$ low-spin state of Ru lies 6308 $cm^{-1}$ above the high-spin $4d^7(^4F)5s^1$, $^5F$ ground state.[55] Similarly, the $4d^7(^4P)5s^1$, $^3P$ low-spin state lies 5191 $cm^{-1}$ above the $4d^7(^4P)5s^1$, $^5P$ high-spin state.[55] These exchange splittings are at least comparable to the predicted $^1\Delta_2$–$^3\Delta_2$ splitting of 4350 $cm^{-1}$, and verify that it lies within the expected range. Although neither the $^3\Delta_1$ nor the $^1\Delta_2$ states are observed in this work, these predictions also provide a useful estimate of the energies of these states. Dispersed fluorescence experiments are currently in progress in this laboratory in the hope of locating these states.

The assignment of the $[0.1]^3\Delta_3$ state as

$10\sigma^2 11\sigma^2 5\pi^4 2\delta^3 12\sigma^1$, $^3\Delta_3$ allows the measured hyperfine parameter for this state, $h\Omega = -0.09\ \mathrm{cm}^{-1}$ for $^{101}Ru^{12}C$, to be used to estimate the amount of $5s_{Ru}$ character in the $12\sigma$ orbital. This state may be represented by a single Slater determinant as

$$\Psi(^3\Delta_3) = |2\delta_{+2}(1)\alpha(1)2\delta_{+2}(2)\beta(2)2\delta_{-2}(3)\alpha(3) \times 12\sigma_0(4)\alpha(4)|, \quad (4.1)$$

allowing Eq. (3.8) to be used to estimate the hyperfine parameter, $h$. After the terms that cancel in Eq. (3.8) are deleted, one obtains the expression

$$h(^3\Delta_3) = [a_{2\delta}\cdot 2 + (b_{F,12\sigma} + b_{F,2\delta} + \tfrac{2}{3}c_{2\delta})\cdot \tfrac{1}{2}], \quad (4.2)$$

which may be approximated using values of $a$, $b_F$, and $c$ based on atomic data. The atomic parameters[56] of $a_{4d}^{01} = -0.004\ 48\ \mathrm{cm}^{-1}$, $a_{4d}^{10} = 0.002\ 12\ \mathrm{cm}^{-1}$, $a_{5s}^{10} = -0.055\ 44\ \mathrm{cm}^{-1}$, and $a_{4d}^{12} = -0.003\ 47\ \mathrm{cm}^{-1}$ correspond to the values of $a_{2\delta}$, $b_{F,2\delta}$, $b_{F,12\sigma}$, and $\frac{2}{3}c_{2\delta}/\langle 3\cos^2\theta - 1\rangle$, assuming that the $2\delta$ and $12\sigma$ orbitals are purely $4d\delta_{Ru}$ and $5s_{Ru}$ in character, respectively. While this assumption is excellent for the $2\delta$ orbital, the $12\sigma$ orbital undoubtedly contains contributions from other atomic orbitals. Since the expression for $h(^3\Delta_3)$ is dominated by the value of $b_{F,12\sigma}$ we can take such orbital mixing into account by introducing a factor, $x$, which describes the amount of $5s_{Ru}$ character in the $12\sigma$ orbital. Thus we finally obtain

$$\begin{aligned} h(^3\Delta_3) &= [-0.004\ 48\cdot 2 + \{-0.055\ 44\cdot x + 0.002\ 12 \\ &\quad + \tfrac{2}{3}\cdot\tfrac{3}{2}(-0.003\ 47)(-\tfrac{4}{7})\}\cdot\tfrac{1}{2}]\ \mathrm{cm}^{-1} \\ &= [-0.006\ 91 - 0.027\ 72\cdot x]\ \mathrm{cm}^{-1}. \end{aligned} \quad (4.3)$$

Equating this to the measured value, $h(^3\Delta_3) = -0.030 \pm 0.003\ \mathrm{cm}^{-1}$, we obtain $x = 0.83 \pm 0.11$. Thus, the $12\sigma$ orbital has roughly 83% $5s_{Ru}$ character, an amount which is consistent with previous estimates for the $12\sigma$ orbital of RhC ($\sim$69% $5s_{Rh}$) (Ref. 25) and for the analogous $9\sigma$ orbital of CoC (89% $4s_{Co}$).[4]

The ground $X\ ^1\Sigma^+$ state of RuC has $r_0 = 1.608$ Å, which compares to $r_0 = 1.635$ Å for the $^3\Delta_i$ state. Although the $12\sigma$ orbital is nominally nonbonding, occupation of this orbital nevertheless causes an increase in bond length by 0.027 Å in RuC. A similar effect has been previously found in CoC, where the $1\delta^4 9\sigma^1$, $X\ ^2\Sigma^+$ state bond length of $r_0 = 1.561$ Å increases by 0.081 Å to $r_0 = 1.642$ Å when a $1\delta$ electron is moved to the $9\sigma$ orbital to produce the $1\delta^3 9\sigma^2$, $^2\Delta_{5/2}$ state.[4] Such an effect is perhaps not surprising when it is noted that the $9\sigma$ (or $12\sigma$) orbital has an apparent metal-based *ns* content of more than 80%. The lack of significant atomic orbital mixing into the $9\sigma$ or $12\sigma$ orbital demonstrates that it is not strongly polarized away from the M–C bond, leading to Pauli repulsions with the bonding $\sigma$ orbital that force the bond length to increase.

### B. Upper states of the observed band systems: $2\delta^3 6\pi^1$, $^{1,3}\Pi$, and $^{1,3}\Phi$ states

From the previous section it is clear that the $[\ldots]2\delta^4$, $^1\Sigma^+$ and $[\ldots]2\delta^3 12\sigma^1$, $^3\Delta$ states are very low in energy and that the $[\ldots]2\delta^3 12\sigma^1$, $^1\Delta_2$ state most likely lies at an energy of about 5000 $\mathrm{cm}^{-1}$. The other low-lying configuration which might be expected is $[\ldots]2\delta^2 12\sigma^2$, leading to $^3\Sigma_{0^+}^-$, $^3\Sigma_1^-$, $^1\Sigma_{0^+}^+$, and $^1\Gamma_4$ states. Apart from the $^1\Sigma_{0^+}^+$ state, none of these upper states are spectroscopically accessible from the $[\ldots]2\delta^4$, $^1\Sigma^+$ or $[\ldots]2\delta^3 12\sigma^1$, $^3\Delta$ states populated in the present study unless the $\Delta S = \Delta\Sigma = 0$, $\Delta\Lambda = \pm 1,0$ selection rules are compromised by substantial spin–orbit mixing. In addition, the $[\ldots]2\delta^2 12\sigma^2$, $^1\Sigma_{0^+}^+$ state is only accessible if configuration interaction is important enough to make two-electron transitions possible. Furthermore, since no upper states with $\Omega = 0$ are observed in this work, it is clear that we are accessing neither the $[\ldots]2\delta^2 12\sigma^2$, $^1\Sigma_{0^+}^+$ nor the $^3\Sigma_{0^+}^-$ states. On this basis these expected low-lying states may be excluded from further consideration.

Apart from the $[\ldots]2\delta^2 12\sigma^2$ configuration, the lowest energy electron configuration not yet considered is the $[\ldots]2\delta^3 6\pi^1$ configuration, which gives rise to $^3\Pi_{0,1,2}$, $^3\Phi_{2,3,4}$, $^1\Pi_1$, and $^1\Phi_3$ electronic terms. The observed upper states lying in the range from 12 700 to 18 090 $\mathrm{cm}^{-1}$ correspond to $\Omega = 2,3,4,1,3,1$, in order of increasing energy, with the last two states lying substantially above the first four. This closely corresponds to what might be expected for the $^{1,3}\Pi$ and $^{1,3}\Phi$ states arising from the $[\ldots]2\delta^3 6\pi^1$ configuration. For such a configuration the $^3\Pi$ and $^3\Phi$ states will lie low in energy, and the $^1\Pi$ and $^1\Phi$ states higher in energy, with singlet–triplet splittings comparable to the exchange splitting in the free atom, which lies in the range of 4000–6000 $\mathrm{cm}^{-1}$. On this basis it seems likely that the $[18.1]^1\Pi_1$ and $[16.2]^1\Phi_3$ states are the $[\ldots]2\delta^3 6\pi^1$, $^1\Pi$ and $^1\Phi$ states, respectively, and that the lower energy $\Omega = 2$, 3, 4, and 1 states are spin–orbit components of the $^3\Pi_{0,1,2}$ and $^3\Phi_{2,3,4}$ states.

Supporting this assignment is the fact that the $[18.1]^1\Pi_1$ state is accessed with much greater intensity from the $X\ ^1\Sigma^+$ state than from the $[0.9]^3\Delta_2$ state, consistent with the $[18.1]^1\Pi_1 \leftarrow X\ ^1\Sigma^+$ transition being spin-allowed and the $[18.1]^1\Pi_1 \leftarrow [0.9]^3\Delta_2$ transition being spin-forbidden. On this basis the $[18.1]^1\Pi_1$ state is assigned as the $[\ldots]2\delta^3 6\pi^1$, $^1\Pi$ state.

Regardless of its parentage, the $[16.2]^1\Phi_3$ state can only be accessed from the $[0.1]^3\Delta_3$ or $[0.9]^3\Delta_2$ states, and more importantly, it can only fluoresce to these states or to the much higher energy $^1\Delta_2$ state, expected near 5200 $\mathrm{cm}^{-1}$. Thus, the considerably longer fluorescence lifetime measured for the $[16.2]^1\Phi_3$ state (0.44 $\mu$s as opposed to 0.18 $\mu$s for the $[18.1]^1\Pi_1$ state) is consistent with a state which is forced to fluoresce either along a spin-forbidden pathway or along a pathway with a substantially reduced $\nu^3$ factor in the expression for the radiative rate. In this case, the $[16.2]^1\Phi_3$ state is thought to be primarily $^1\Phi_3$ in character, with fluorescence occurring primarily to the $^1\Delta_2$ state. In addition, fluorescence may occur to the $^3\Delta_2$ state due to spin–orbit mixing of $^3\Phi_3$ character into the $[16.2]^1\Phi_3$ state, as discussed in the next section. These assignments of the $[18.1]^1\Pi_1$ and $[16.2]^1\Phi_3$ states as the $[\ldots]2\delta^3 6\pi^1$, $^1\Pi_1$ and $^1\Phi_3$ states, respectively, predict that fluorescence from these states will occur mainly to the $X\ ^1\Sigma^+$ and $^1\Delta_2$ states, respectively. These predictions are currently being tested by dispersed fluorescence studies.

To lower energies one finds the $[12.7]^3\Pi_2$, $[13.5]^3\Phi_3$, $[13.9]^3\Phi_4$, and $[13.9]^3\Pi_1$ states, respectively. Assuming that these may be assigned to the $[\ldots]2\delta^3 6\pi^1$, $^3\Pi_{0,1,2}$ and $^3\Phi_{2,3,4}$ levels, one is forced to conclude that the $[13.5]^3\Phi_3$, $[13.9]^3\Phi_4$, and $[13.9]^3\Pi_1$ states correspond to the $^3\Phi_3$, $^3\Phi_4$, and $^3\Pi_1$ states, respectively. In principle, the $[12.7]^3\Pi_2$ state could correspond to either the $^3\Pi_2$ or $^3\Phi_2$ state, but the great intensity of the $[12.7]^3\Pi_2 \leftarrow [0.1]^3\Delta_3$ system in absorption and especially in emission argues for the assignment of the $[12.7]^3\Pi_2$ state as $^3\Pi_2$. This is because a $[12.7]^3\Pi_2 \leftarrow [0.1]^3\Delta_3$ system obeys the $\Delta\Sigma = 0$ selection rule, while the alternative $[12.7]^3\Phi_2 \leftarrow [0.1]^3\Delta_3$ assignment corresponds to a forbidden $\Delta\Sigma = -2$ transition, and is not expected to be observed.

#### 1. Spin–orbit structure of the excited $2\delta^3 6\pi^1$ states

Testing these ideas, we note that the methods described by Lefebvre-Brion and Field[48] allow the spin–orbit splitting, $A\Lambda$, for the $[\ldots]2\delta^3 6\pi^1$, $^3\Pi$ and $^3\Phi$ states to be calculated as $A\Lambda = -a_\delta - a_\pi/2$ and $A\Lambda = -a_\delta + a_\pi/2$, respectively. Assuming that the $2\delta$ and $6\pi$ orbitals are primarily composed of $4d_{\mathrm{Ru}}$ atomic orbitals, this leads to $A\Lambda = -3/2\zeta_{4d}(\mathrm{Ru}) \approx -1557\ \mathrm{cm}^{-1}$ and $A\Lambda = -1/2\zeta_{4d}(\mathrm{Ru}) \approx -519\ \mathrm{cm}^{-1}$ for the $^3\Pi$ and $^3\Phi$ states, respectively, using $\zeta_{4d}(\mathrm{Ru}) = 1038\ \mathrm{cm}^{-1}$.[48] Thus, the $^3\Pi$ state is predicted to be strongly inverted, consistent with the measured separation between the $[13.9]^3\Pi_1$ and $[12.7]^3\Pi_2$ states of $1211\ \mathrm{cm}^{-1}$. The fact that this separation is of smaller magnitude than the predicted value of $1557\ \mathrm{cm}^{-1}$ is no cause for concern, since in the $6\pi$ orbital the $4d\pi_{\mathrm{Ru}}$ character is diluted by the admixture of carbon $2p\pi$ character, thereby reducing the expected spin–orbit splitting. In addition, off-diagonal spin–orbit interactions between the $^1\Pi_1$ and $^3\Pi_1$ states will push the $^3\Pi_1$ state to lower energies, further reducing the measured $^3\Pi_1$–$^3\Pi_2$ interval. Additional support for the assignment of the $[12.7]^3\Pi_2$ and $[13.9]^3\Pi_1$ states as spin–orbit levels of a common $^3\Pi$ state is found in their similar bond lengths (with $r_e$ values differing by only 0.0008 Å) and vibrational frequencies (which differ in $\omega_e$ by only $9.5\ \mathrm{cm}^{-1}$, or 1%).

Although the spin–orbit analysis presented above predicts that the $^3\Phi$ state will be less strongly inverted than the $^3\Pi$ state, with $A\Lambda \approx -519\ \mathrm{cm}^{-1}$, it is nevertheless still predicted to be inverted. This is at odds with the measured spectra, which place the $[13.9]^3\Phi_4$ state $421\ \mathrm{cm}^{-1}$ *above* the $[13.5]^3\Phi_3$ state. The off-diagonal spin–orbit interaction between the isoconfigurational $^1\Phi_3$ and $^3\Phi_3$ states, however, can exert a substantial effect because the spin–orbit matrix element is readily calculated to be $\langle {}^3\Phi_3|\hat{H}^{\mathrm{SO}}|{}^1\Phi_3\rangle = a_\delta + a_\pi/2 \approx 1557\ \mathrm{cm}^{-1}$.[48] Because this value is larger than the diagonal spin–orbit matrix element of $\langle {}^3\Phi_4|\hat{H}^{\mathrm{SO}}|{}^3\Phi_4\rangle = -a_\delta + a_\pi/2 \approx -519\ \mathrm{cm}^{-1}$, spin–orbit coupling between the $^3\Phi_3$ and $^1\Phi_3$ states may be responsible for the reversed energy ordering of the $^3\Phi_3$ and $^3\Phi_4$ states. This possibility requires a small exchange splitting between the $^1\Phi$ and $^3\Phi_3$ states.

The measured splitting between the states assigned as $^3\Phi_3$ and $^1\Phi_3$ is $2720.4\ \mathrm{cm}^{-1}$, a value which is even less than the expected minimum splitting between the final mixed states of $2 \times \langle {}^3\Phi_3|\hat{H}^{\mathrm{SO}}|{}^1\Phi_3\rangle \approx 3114\ \mathrm{cm}^{-1}$. This implies that the off-diagonal spin–orbit matrix element is smaller than $1557\ \mathrm{cm}^{-1}$, a fact that is not unreasonable given that the $6\pi$ orbital is not purely $4d\pi_{\mathrm{Ru}}$ in character. It also implies that in the absence of spin–orbit interaction the $^3\Phi_3$ and $^1\Phi_3$ states lie very close in energy, so that the state we have designated as $^3\Phi_3$ is lowered substantially when spin–orbit interaction is considered. With a coupling matrix element of 1000–1500 $\mathrm{cm}^{-1}$ a lowering of the $^3\Phi_3$ level by over 1000 $\mathrm{cm}^{-1}$ could easily occur. This would be more than sufficient to account for the reversal in energy ordering of the $^3\Phi_3$ and $^3\Phi_4$ states. Of course, an additional consequence of this coupling is that the states we have labeled as $^3\Phi_3$ and $^1\Phi_3$ are in reality very strongly mixed.

#### 2. Hyperfine structure of the excited $2\delta^3 6\pi^1$ states

The methods used in Sec. IV A to predict the hyperfine parameter, $h$, for the $[0.1]^3\Delta_3$ level may also be applied to the other observed levels. Again using the known atomic hyperfine parameters,[56] expected values of $h$ for the $[0.9]^3\Delta_2$ and $[\ldots]2\delta^3 12\sigma^1$, $^1\Delta_2$ levels of $h = -0.009\ \mathrm{cm}^{-1}$ are obtained. This is not too far outside of our experimental estimate for the $[0.9]^3\Delta_2$ state of $0.000 \pm 0.005\ \mathrm{cm}^{-1}$ (see Table III).

Estimates of $h$ for the excited states thought to derive from the $[\ldots]2\delta^3 6\pi^1$ configuration work out to be $-0.013$, $-0.013$, and $-0.002\ \mathrm{cm}^{-1}$ for the $[16.2]^1\Phi_3$, $[13.5]^3\Phi_3$, and $[12.7]^3\Pi_2$ states, respectively, under the assumption that the $6\pi$ orbital is of pure $4d\pi_{\mathrm{Ru}}$ character. These values compare to experimental estimates of $-0.018(3)$, $0.000(3)$, and $+0.008(5)\ \mathrm{cm}^{-1}$, respectively. The calculated and experimental estimates for the $[16.2]^1\Phi_3$ state are in reasonable agreement, but a greater discrepancy exists for the $[13.5]^3\Phi_3$ and $[12.7]^3\Pi_2$ states. This discrepancy suggests that it is not possible to accurately describe these excited states as arising from a single configuration. Both spin–orbit mixing (such as certainly occurs between the $[16.2]^1\Phi_3$ and $[13.5]^3\Phi_3$ states) and configurational mixing due to electron correlation can cause $h$ to deviate from the simple estimates given above. Spin–orbit mixing of the $[16.2]^1\Phi_3$ and $[13.5]^3\Phi_3$ states can be accounted for rather straightforwardly, since the coupling matrix element is readily calculated as $\langle {}^3\Phi_3|\hat{H}^{\mathrm{SO}}|{}^1\Phi_3\rangle = a_\delta + a_\pi/2 \approx 1557\ \mathrm{cm}^{-1}$. The measured energies of the $[16.2]^1\Phi_3$ and $[13.5]^3\Phi_3$ states, however, are inconsistent with values of $\langle {}^3\Phi_3|\hat{H}^{\mathrm{SO}}|{}^1\Phi_3\rangle$ greater than $1360\ \mathrm{cm}^{-1}$ unless additional perturbations are considered. These facts imply that the $^1\Phi_3$ and $^3\Phi_3$ states are severely mixed, so that each has considerable $S=0$ and $S=1$ electronic character. Assuming that the mixing is complete and using the hyperfine parameters of Büttgenbach[56] then leads to revised estimates of $h$ for these states of $-0.015$ and $-0.012\ \mathrm{cm}^{-1}$, respectively. This brings the theoretical estimates of $h$ into slightly better agreement with the experimental values of $-0.018(3)$ and $0.000(3)$, respectively. Clearly additional mixing of states due to the spin–orbit interaction or electron correlation is needed to explain the observed hyperfine structure of the $\Omega = 3$ states.

The difficulties are even more severe for the $[12.7]^3\Pi_2$ state, which our experiments clearly show possesses a positive value of $h$, but which is calculated to have a negative expected value of $-0.002\ \mathrm{cm}^{-1}$. This again suggests that the $[12.7]^3\Pi_2$ state is contaminated, either by spin–orbit mixing or configuration interaction with another state.

#### 3. Previous observations of the excited $2\delta^3 6\pi^1$ states

In the original spectroscopic study of RuC, Scullman and Thelin observed 8 band systems in emission, with origin bands in the range from 12 624 to 15 345 $\mathrm{cm}^{-1}$.[39] The systems reported in that work were completely consistent with the assignments made above, with all of the observed systems corresponding to allowed $\Delta S=\Delta\Sigma=0$ emissions except for the weakest of the observed systems, which corresponds in our assignment to a spin-forbidden $[16.2]^1\Phi_3 \rightarrow [0.9]^3\Delta_2$ emission. It is not surprising that this system is observed in emission, since our estimate of the $^1\Phi_3 \sim {}^3\Phi_3$ matrix element of $\langle {}^3\Phi_3|\hat{H}^{\mathrm{SO}}|{}^1\Phi_3\rangle \approx 1557\ \mathrm{cm}^{-1}$ leads to a nearly complete mixing of the $^1\Phi_3$ and $^3\Phi_3$ states.

In addition to the emission systems also observed in our work, Scullman and Thelin identified three other band systems with origin bands at 12 875.23, 13 286.43, and 13 312.69 $\mathrm{cm}^{-1}$.[39] Because this early work was not isotopically resolved, it was only possible to rotationally resolve the 0–0 bands of these systems. Nevertheless, the three systems were found to have $B_0''$ values of 0.5882(4), 0.5882(5), and 0.5887(9) $\mathrm{cm}^{-1}$. These values are statistically the same, and are statistically different from the $B_0$ values found for the $X\ ^1\Sigma^+$, $[0.1]^3\Delta_3$, and $[0.9]^3\Delta_2$ states. Nevertheless, they are very close to the isotopically averaged values found by Scullman and Thelin for the $[0.1]^3\Delta_3$ and $[0.9]^3\Delta_2$ states, which are 0.5863 and 0.5877 $\mathrm{cm}^{-1}$, respectively. It therefore seems very likely that these emission systems terminate on the $^3\Delta_1$ level, which is not observed in our work due to its low population in the jet-cooled molecular beam. Assuming that these emission systems obey the $\Delta S=\Delta\Sigma=0$ selection rule and that they originate from the $[\ldots]2\delta^3 6\pi^1$ manifold of states, the only candidates which can emit to the $^3\Delta_1$ level are the $^3\Phi_2$, $^3\Pi_{0^+}$, and $^3\Pi_{0^-}$ states. It therefore appears that these three band systems are the $^3\Phi_2 \rightarrow {}^3\Delta_1$, $^3\Pi_{0^+} \rightarrow {}^3\Delta_1$, and $^3\Pi_{0^-} \rightarrow {}^3\Delta_1$ emission systems.

If one assumes that the spin–orbit structure of the $[\ldots]2\delta^3 6\pi^1$, $^3\Pi$ state exhibits equal spacing between the $^3\Pi_2$, $^3\Pi_1$, and $^3\Pi_{0^\pm}$, levels, the $^3\Pi_{0^\pm}$ levels would be expected to lie at 15 156 $\mathrm{cm}^{-1}$. Given that the $^3\Pi_1$ level is pushed to lower energies by an isoconfigurational spin–orbit interaction with the $[\ldots]2\delta^3 6\pi^1$, $^1\Pi_1$ state, however, the $^3\Pi_{0^\pm}$ levels might more realistically be expected to lie at $T_0({}^3\Pi_2)+2|A|\Lambda = 12\,734+2(1557)=15\,848\ \mathrm{cm}^{-1}$. Similar calculations suggest that the $^3\Phi_2$ level should lie in the energy range of 13 900–14 900 $\mathrm{cm}^{-1}$. These considerations clearly place the $^3\Phi_2$ level below the $^3\Pi_{0^\pm}$ levels. Furthermore, the $^3\Pi_{0^\pm}$ levels are expected to lie close to one another, because they are split only by second-order spin–orbit interactions with other $\Omega=0$ states. These facts suggest that the band systems with origin bands at 13 286.43 and 13 312.69 $\mathrm{cm}^{-1}$ are the $^3\Pi_{0^\pm} \rightarrow {}^3\Delta_1$ systems, with the $^3\Pi_{0^\pm}$ levels split by 26.26 $\mathrm{cm}^{-1}$. The lower energy system, with its origin at 12 875.23 $\mathrm{cm}^{-1}$, then most probably is the $^3\Phi_2 \rightarrow {}^3\Delta_1$ emission system. With these thoughts in mind the $^3\Delta_1$, $^3\Phi_2$, $^3\Pi_{0a}$, and $^3\Pi_{0b}$ levels are listed in Table III at the term energies $x$, $x+12\,875.23\ \mathrm{cm}^{-1}$, $x+13\,286.43\ \mathrm{cm}^{-1}$, and $x+13\,312.69\ \mathrm{cm}^{-1}$, respectively. Based on the spin–orbit considerations discussed in Sec. IV A, it is expected that $x$ should fall in the range from 1620 to 2150 $\mathrm{cm}^{-1}$. This places the $^3\Phi_2$, $^3\Pi_{0a}$, and $^3\Pi_{0b}$ levels at energies which are completely consistent with the expected values given above. We are thus led to conclude that the weak but nevertheless power broadened feature that was observed in the course of scanning the 1–1 band of the $[13.5]^3\Phi_3 \leftarrow [0.1]^3\Delta_3$ system, as described in Sec. III B 2, is due to an overlapping transition that is probably the 0–0 band of the $^3\Pi_{0b} \leftarrow {}^3\Delta_1$ system. Because the $[13.5]^3\Phi_3 \leftarrow [0.1]^3\Delta_3$ system fails to follow the $\Delta\Sigma=0$ selection rule, it is a weak system which is not readily power broadened. The $^3\Pi_{0b} \leftarrow {}^3\Delta_1$ system, on the other hand, is fully allowed under the $\Delta\Sigma=0$ selection rule, and is readily power broadened under the conditions required to record the weaker overlapping band.

### C. Comparison with *ab initio* calculations

The only *ab initio* study of RuC published at this time consists of a 1987 all-electron Hartree–Fock and configuration interaction calculation by Shim *et al.*[34] This study predicted a $^3\Delta$ ground state, with $r_e=1.74$ Å, $\omega_e=888\ \mathrm{cm}^{-1}$, and $D_e=2.92$ eV. The bond length for this state is overestimated by 0.1 Å, $\omega_e$ is underestimated by 15%, and $D_e$ is underestimated by a factor of 2 in this calculation. In addition, the $^1\Sigma^+$ state that has now been established as the ground state is calculated to lie 4275 $\mathrm{cm}^{-1}$ above the $^3\Delta$ state. Clearly, the theoretical methods employed in this calculation were inadequate to describe RuC. A more recent *ab initio* investigation of the closely related MoC molecule by these same authors which employed an all electron multiconfigurational self-consistent field method (CASSCF) followed by multireference configuration interaction (MRCI) calculations was much more successful, reproducing the experimental MoC ground state bond length[8] to within 0.02 Å and the dissociation energy to within 4%.[33] These results suggest that multiconfigurational self-consistent field methods will generally be required for an accurate description of the electronic structure of the transition metal carbides.

The *ab initio* study of RuC by Shim *et al.*[34] was used to estimate the thermodynamic functions of RuC, which were then used to extract the value $D_0(\mathrm{RuC})=6.34\pm0.11$ eV from the results of Knudsen effusion mass spectrometric experiments.[34] A recalculation of the thermodynamic functions of RuC using the results listed in Table III for the low-lying states leads to a slight revision in this value. With the new data $D_0(\mathrm{RuC})$ is revised to $6.31\pm0.11$ eV.

## V. CONCLUSION

In our recent work on FeC,[3] NiC,[12] and MoC (Ref. 8) we have found that these molecules possess vibronic spectra of nearly impenetrable complexity, making even the identification of band systems very difficult. The situation in RuC is

exactly the opposite. The observed band systems are readily identified, with isotope shifts and rotational constants that vary in precisely the expected manner with $v'$. The stronger bond in RuC, as compared to FeC and NiC, probably accounts for the simplicity of its spectrum compared to these molecules; a larger orbital splitting in RuC implies a reduced density of states, making for a simpler, more readily interpreted spectrum.

Through the present investigation, which builds heavily on the pioneering work of Scullman and Thelin, the $2\delta^4$, $X\ ^1\Sigma^+$; $2\delta^3 12\sigma^1$, $^3\Delta_{2,3}$; $2\delta^3 6\pi^1$, $^3\Pi_{1,2}$; $2\delta^3 6\pi^1$, $^3\Phi_{3,4}$; $2\delta^3 6\pi^1$, $^1\Phi_1$; and $2\delta^3 6\pi^1$, $^1\Pi_1$ states have been thoroughly characterized and placed on a common energy scale. Bond lengths of the various states are well-correlated with their electronic configuration. The $2\delta^4$, $X\ ^1\Sigma^+$ state has $r_0 = 1.608$ Å; the $2\delta^3 12\sigma^1$, $^3\Delta$ state has $r_e = 1.635$ Å, and the various states of the $2\delta^3 6\pi^1$ configuration have $r_e$ in the range from 1.657 to 1.678 Å. Likewise, the vibrational frequency decreases with increasing electronic energy in a manner that parallels the changes in bond length.

An unexpected reversal of the energy ordering of the $\Omega = 3$ and 4 substates of the $2\delta^3 6\pi^1$, $^3\Phi_i$ state likely results from a large isoconfigurational spin–orbit interaction between the $2\delta^3 6\pi^1$, $^3\Phi_3$ and $^1\Phi_3$ states. The off-diagonal spin–orbit matrix element coupling these states is roughly three times the diagonal matrix element which splits them in first order perturbation theory, resulting in an unusual pattern of spin–orbit levels.

Hyperfine splittings in the spectra of the $^{99}Ru^{12}C$ and $^{101}Ru^{12}C$ isotopomers have been analyzed to show that the $12\sigma$ molecular orbital of the $2\delta^3 12\sigma^1$, $^3\Delta_3$ state has $83 \pm 11\% 5s_{Ru}$ character. This is in accord with related measurements on the $1\delta^4 9\sigma^1$, $^2\Sigma^+$ state of CoC (Ref. 4) and the $2\delta^4 12\sigma^1$, $^2\Sigma^+$ state of RhC.[25]

With the addition of this work on RuC, it is now fair to say that the $4d$ transition metal carbides are much better understood than either the $3d$ or $5d$ series. Detailed optical spectra are now published for YC,[6] NbC,[7] MoC,[8] RuC, and RhC (Refs. 14–16) in the $4d$ series, as opposed to just FeC (Refs. 1–3) and CoC (Refs. 4, 5) in the $3d$ series and IrC (Refs. 9, 17, 18) and PtC (Refs. 10, 11, 19–22) in the $5d$ series. To gain a more comprehensive understanding of the differences between the $3d$, $4d$, and $5d$ transition metal carbides, further work will be needed, particularly on the $3d$ and $5d$ metal carbides.

## ACKNOWLEDGMENTS

We thank the U.S. Department of Energy (DE-FG03-93ER143368) for support of this research. We also acknowledge the donors of the Petroleum Research Fund, administered by the American Chemical Society, for partial support of this research. We also thank Professor T. C. Steimle and Dr. B. Simard for helpful comments.

[1] W. J. Balfour, J. Cao, C. V. V. Prasad, and C. X. Qian, J. Chem. Phys. **103**, 4046 (1995).
[2] M. D. Allen, T. C. Pesch, and L. M. Ziurys, Astrophys. J. **472**, L57 (1996).
[3] D. J. Brugh and M. D. Morse, J. Chem. Phys. **107**, 9772 (1997).
[4] M. Barnes, A. J. Merer, and G. F. Metha, J. Chem. Phys. **103**, 8360 (1995).
[5] A. G. Adam and J. R. D. Peers, J. Mol. Spectrosc. **181**, 24 (1997).
[6] B. Simard, P. A. Hackett, and W. J. Balfour, Chem. Phys. Lett. **230**, 103 (1994).
[7] B. Simard, P. I. Presunka, H. P. Loock, A. Berces, and O. Launila, J. Chem. Phys. **107**, 307 (1997).
[8] D. J. Brugh, T. J. Ronningen, and M. D. Morse, J. Chem. Phys. **109**, 7851 (1998), preceding paper.
[9] A. J. Marr, M. E. Flores, and T. C. Steimle, J. Chem. Phys. **104**, 8183 (1996).
[10] T. C. Steimle, K. Y. Jung, and B.-Z. Li, J. Chem. Phys. **102**, 5937 (1995).
[11] T. C. Steimle, K. Y. Jung, and B.-Z. Li, J. Chem. Phys. **103**, 1767 (1995).
[12] D. J. Brugh and M. D. Morse, J. Chem. Phys. (in preparation).
[13] J. D. Langenberg, L. Shao, and M. D. Morse, J. Chem. Phys. (in preparation).
[14] A. Lagerqvist, H. Neuhaus, and R. Scullman, Z. Naturforsch. A **20**, 751 (1965).
[15] A. Lagerqvist and R. Scullman, Ark. Fys. **32**, 475 (1966).
[16] B. Kaving and R. Scullman, J. Mol. Spectrosc. **32**, 475 (1969).
[17] K. Jansson, R. Scullman, and B. Yttermo, Chem. Phys. Lett. **4**, 188 (1969).
[18] K. Jansson and R. Scullman, J. Mol. Spectrosc. **36**, 268 (1970).
[19] H. Neuhaus, R. Scullman, and B. Yttermo, Z. Naturforsch. A **20**, 162 (1965).
[20] R. Scullman and B. Yttermo, Ark. Fys. **33**, 231 (1966).
[21] O. Appelblad, R. F. Barrow, and R. Scullman, Proc. Phys. Soc. London **91**, 260 (1967).
[22] O. Appelblad, C. Nilsson, and R. Scullman, Phys. Scr. **7**, 65 (1973).
[23] R. J. Van Zee, J. J. Bianchini, and W. Weltner, Jr., Chem. Phys. Lett. **127**, 314 (1986).
[24] Y. M. Hamrick and W. Weltner, Jr., J. Chem. Phys. **94**, 3371 (1991).
[25] J. M. Brom, Jr., W. R. M. Graham, and W. Weltner, Jr., J. Chem. Phys. **57**, 4116 (1972).
[26] C. W. Bauschlicher, Jr., and P. E. M. Siegbahn, Chem. Phys. Lett. **104**, 331 (1984).
[27] M. D. Hack, R. G. A. R. Maclagan, G. E. Scuseria, and M. S. Gordon, J. Chem. Phys. **104**, 6628 (1996).
[28] S. M. Mattar, J. Phys. Chem. **97**, 3171 (1993).
[29] R. G. A. R. Maclagan and G. E. Scuseria, Chem. Phys. Lett. **262**, 87 (1996).
[30] I. Shim and K. A. Gingerich, Int. J. Quantum Chem. **42**, 349 (1992).
[31] R. G. A. R. Maclagan and G. E. Scuseria, J. Chem. Phys. **106**, 1491 (1997).
[32] I. Shim, M. Pelino, and K. A. Gingerich, J. Chem. Phys. **97**, 9240 (1992).
[33] I. Shim and K. A. Gingerich, J. Chem. Phys. **106**, 8093 (1997).
[34] I. Shim, H. C. Finkbeiner, and K. A. Gingerich, J. Phys. Chem. **91**, 3171 (1987).
[35] I. Shim and K. A. Gingerich, Surf. Sci. **156**, 623 (1985).
[36] I. Shim and K. A. Gingerich, J. Chem. Phys. **81**, 5937 (1984).
[37] H. Tan, M. Liao, and K. Balasubramanian, Chem. Phys. Lett. **280**, 423 (1997).
[38] H. Tan, M. Liao, and K. Balasubramanian, Chem. Phys. Lett. **280**, 219 (1997).
[39] R. Scullman and B. Thelin, Phys. Scr. **3**, 19 (1971).
[40] R. Scullman and B. Thelin, Phys. Scr. **5**, 201 (1972).
[41] N. S. McIntyre, A. Van Der Anwera-Mathieu, and J. Drowart, Trans. Faraday Soc. **64**, 3006 (1968).
[42] K. A. Gingerich, Chem. Phys. Lett. **75**, 523 (1974).
[43] S. C. O'Brien, Y. Liu, Q. Zhang, J. R. Heath, F. K. Tittel, R. F. Curl, and R. E. Smalley, J. Chem. Phys. **84**, 4074 (1986).
[44] S. Gerstenkorn and P. Luc, *Atlas du Spectre d'Absorption de la Molecule d'Iode Entre* 14 800–20 000 $cm^{-1}$ *(CNRS, Paris, 1978).*
[45] S. Gerstenkorn and P. Luc, Rev. Phys. Appl. **14**, 791 (1979).
[46] S. Gerstenkorn, J. Verges, and J. Chevillard, *Atlas du Spectre d'Absorption de la Molecule d'Iode Entre* 11 000–14 000 $cm^{-1}$ *(CNRS, Paris, 1982).*
[47] J. M. Brown and A. J. Merer, J. Mol. Spectrosc. **74**, 488 (1979).
[48] H. Lefebvre-Brion and R. W. Field, *Perturbations in the Spectra of Diatomic Molecules* (Academic, Orlando, 1986).
[49] See AIP Document No. PAPS JCPSA6-109-014842-67 for 67 pages of absolute line positions, fits of $B_v$ values, and vibronic fits. Order by PAPS number and journal reference from American Institute of Physics, Physics Auxiliary Publication Service, 500 Sunnyside Boulevard, Woodbury, NY

11797-2999. Fax: 516-576-2223, e-mail: paps@aip.org. The price is $1.50 for each microfiche (48 pages) or $5.00 for photocopies up to 30 pages, and $0.15 for each additional page over 30 pages. Airmail additional. Make checks payable to the American Institute of Physics.

[50] W. Weltner, Jr., *Magnetic Atoms and Molecules* (Dover, New York, 1983).

[51] R. A. Frosch and H. M. Foley, Phys. Rev. **88**, 1337 (1952).

[52] T. M. Dunn, in *Molecular Spectroscopy: Modern Research*, edited by K. N. Rao and C. W. Mathews (Academic, New York, 1972), p. 231.

[53] C. H. Townes and A. L. Schawlow, *Microwave Spectroscopy* (Dover, New York, 1975).

[54] C. L. Callender, P. A. Hackett, and D. M. Rayner, J. Opt. Soc. Am. B **5**, 614 (1988).

[55] C. E. Moore, *Table of Atomic Energy Levels*, Natl. Bur. Stand. (U.S. GPO, Washington, D.C., 1971).

[56] S. Büttgenbach, *Hyperfine Structure in* $4d$- *and* $5d$-*Shell Atoms* (Springer, Berlin, 1982).